JOURNAL OF CATALYSIS 39, 234–248 (1975)

Study of Copper–Nickel Alloy Formation on Silica Supports by the Magnetostatic and Other Methods

S. D. ROBERTSON, S. C. KLOET AND W. M. H. SACHTLER

Koninklijke/Shell-Laboratorium, Amsterdam (Shell Research B.V.), Badhuisweg 3, Amsterdam-N., The Netherlands

Received November 18, 1974

Magnetostatic and resonance methods have demonstrated the formation of alloys in several silica-supported copper–nickel systems whose metal loadings were varied between 1 and 10% wt. The preparations studied were obtained by impregnation, ion exchange and coprecipitation techniques. In most systems the metals were believed to be reduced but for samples prepared by impregnation with a metal sulfate some sulfide formation was indicated. In all the bimetallic samples the composition of the alloy particles was found to be nonuniform. The two-phase "cherry" model demonstrated for large particles at temperatures and compositions where the Cu–Ni system is characterized by a miscibility gap, is not found applicable to the much smaller particles in supported Cu–Ni catalysts. Incorporation of a calcination step or reduction of the surface area of the support lowered the degree of dispersion but led to more homogeneous alloys.

The conclusions from the magnetic data were confirmed and augmented by X-ray diffraction results, which demonstrated for the precalcined preparations a preferential copper oxide reduction. It is also shown that the preparation of fairly homogeneous supported copper–nickel alloys is assisted by using high relative nickel loadings in those cases where there is an enhanced oxide miscibility prior to reduction.

I. INTRODUCTION

Bimetallic catalysts are a subject of considerable interest in catalysis research because the selectivity of the bimetal species differs markedly from that of their components. For example, the selectivity of silver in the oxidation of ethylene to ethylene oxide (*1*) (as opposed to carbon dioxide and water) and of cumene to cumene hydroperoxide (*2*) is increased remarkably by alloying with gold, yet the latter is itself inactive in these reactions. Similarly, alloying nickel with copper clearly modifies the activity of the former metal in the hydrogenation of ethylene (*3,4*), benzene (*5,6*) and butadiene (*7*). This alloy system has also demonstrated a remarkable selectivity in the isomerization, as opposed to hydrogenolysis, of *n*-hexane though copper itself is virtually inactive (*8*).

The majority of these studies have been made on unsupported bimetallic systems (films or powders), where the nature of alloying can be judged by physical methods of structural analysis such as X-ray diffraction. The constitution of supported copper–nickel systems has also been examined in this way (*9,10*) but the X-ray method fails to provide such information on catalysts with a low metal loading, where the metal particles are often smaller than 3.0 nm. The nature of the interactions taking place in supported bimetallic systems cannot therefore be determined readily by such direct methods of

structural analysis. Systems of this type have also presented analytical difficulties in the application of techniques of Auger and X-ray photoelectron spectroscopy; nevertheless, some work has been done in this field (*11,12*).

In view of these complexities a magnetostatic (and resonance) study was made of bimetallic systems where the two metal components and the alloy have different magnetic properties. The copper–nickel system was chosen as one model, since it is in many ways ideally suited to such magnetic work. The extreme sensitivity of nickel ferromagnetism to applied fields can be exploited, as can the large decrease of this ferromagnetism upon alloying with (diamagnetic) copper, especially in copper-rich compositions (*13*). Clearly, these alloys are magnetically distinguishable from their components since, when nonalloyed, nickel exhibits a saturation magnetization of 57 emu/g at all compositions. This distinction remains possible for supported catalysts. The field dependence of the specific magnetization of highly dispersed ferromagnetic materials differs, however, from that of the nondispersed system and is conventionally described as "superparamagnetic" (*14*), i.e., each particle acts as a single magnetic domain where all the atomic magnetic moments are cooperatively aligned.

Such domains (assumed spherical) are less than about 30.0 nm in diameter (*15*), typical of nickel in the supported catalysts studied. Such a particle may be thought of as a paramagnetic "atom" of very large magnetic moment. An applied field, H, tends to orientate these monodomain particles but their ability to achieve complete alignment with the field and, hence, acquire a limiting or "saturation" magnetization is, however, hindered by thermal agitation at any temperature above absolute zero. Thus the observed magnetization will be lower than the saturation value as given by the Langevin function

$$\frac{\sigma}{\sigma_s} = \coth \frac{\mu H}{kT} - \frac{kT}{\mu H}, \qquad (1)$$

where σ specific magnetization at H and T,
σ_s specific magnetization at saturation,
H applied field,
T absolute temperature,
k Boltzmann constant,
μ magnetic moment of particle.

The significance of such superparamagnetic behavior for the detection of finely dispersed alloying is that, at any temperature above absolute zero, the specific magnetization of the nickel in the bimetallic catalysts must be compared with that of the corresponding nickel-only standard.

As the surface-to-volume ratio of supported nickel catalysts is very high, the decrease of their magnetization on hydrogen adsorption can be readily measured (*14,16*). This additional feature of supported-nickel magnetization may also be used to identify the nickel surface area in bimetallic catalysts.

Copper–nickel alloys with macroscopic particles can exist in equilibrium either as a continuous series of solid solutions or as a two-phase system, where a copper-rich alloy envelops crystals of a nickel-rich alloy (i.e., the "cherry" model) (*17,18*). For macroscopic systems the latter model is stable at temperatures below ca. 320°C, whereas solid solutions are stable above this temperature (*19*).

For highly dispersed systems, however, it is not justified to accept the validity of the cherry model without special proof, because for small particles the additional surface energy of a two-phase arrangement may be too high (*20*). It is, therefore, advantageous that the two arrangements might be distinguished by a magnetic method, the cherry arrangement having a higher magnetization—due to the nickel-rich core—than the solid solution. Additional information which might aid the dis-

crimination between the two models can be obtained by measuring the change in magnetization caused by hydrogen adsorption. In the case of the cherry arrangement, hydrogen adsorption on a diamagnetic copper-rich surface should not cause a measurable change in magnetization, but such a change would be expected for superparamagnetic systems with particles of equal bulk and surface compositions.

II. METHODS

1. Measurement of Specific Magnetizations by the Faraday Method

Nickel specific magnetizations (σ) can be obtained from the relation

$$\sigma = \chi \cdot H, \qquad (2)$$

where χ = mass susceptibility (cc/g), H = field strength [Oe (1 oersted = $10^3/4\pi$A m^{-1})].

There are two classical approaches for measuring mass susceptibility, namely the Gouy and the Faraday method. The latter technique was preferred as it offers several advantages in the study of powder samples such as catalysts (*21,22*). The Faraday method, moreover, lends itself to *in situ* studies of changes in magnetization on gas adsorption. Figure 1 displays the apparatus used, where the magnetic properties of (*in situ*) reduced catalysts in a high vacuum system [10^{-6}Torr (1 Torr = 133.322 N m^{-2})] equipped with an ultramicrobalance (Sartorius Electrono I) were measured by an electromagnet (0–10 kOe field strength). Standard procedures were employed for calibrating the system and measuring the mass susceptibility (*23*).

The applied field was estimated by a calibrated Hall probe. An apparent saturation magnetization of 54.50 emu/g Ni at 293 K was derived from extrapolating the measured specific magnetizations of a nickel powder to zero reciprocal field. This corresponded closely with that of bulk nickel (54.39 emu/g Ni).

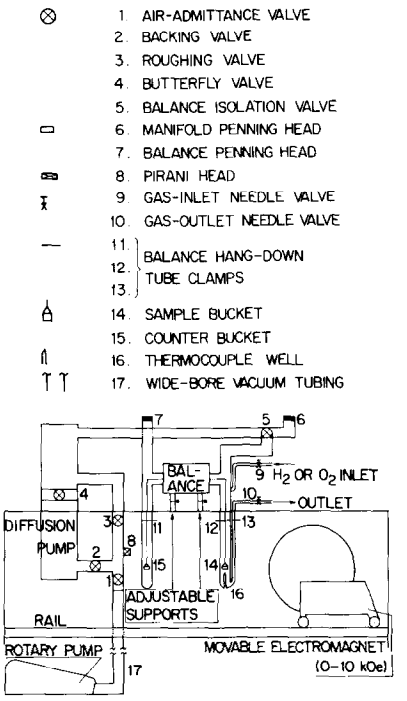

FIG. 1. Magnetostatic (Faraday) apparatus.

Silica-supported catalysts were used for they favor the assumption of minimal metal–carrier interaction implicit in applying Wiedemann's additivity law:

$$\chi_{\text{catalyst}} = P_{SiO2}\,\chi_{SiO2} + P_{Ni}\chi_{Ni} + P_{Cu}\chi_{Cu}, \qquad (3)$$

where P and χ correspond, respectively, to the weight fraction and mass susceptibility of each component. In the low-loaded copper–nickel catalysts studied the copper contribution to the overall susceptibility can be neglected because of its very weak diamagnetism. The entire catalyst sample employed in the magnetic measurements was subsequently analyzed using atomic absorption spectroscopy to overcome any problems of heterogeneity of metal distribution.

More detailed information on the nickel specific magnetization at low-field strengths (max 800 Oe) was obtained from an induction-coil apparatus (*24*). The Langevin function can be modified (*25*) to give such a low-field (initial slope) estimate

of the average crystallite volume $\bar{v}^2/\bar{v}$, viz,

$$\frac{\bar{v}^2}{\bar{v}} = \frac{3kT}{I_{sp}H} \cdot \frac{\sigma}{\sigma_s}, \qquad (4)$$

where K, T, σ, σ_s, and H are as in Eq. (1) and I_{sp} is the spontaneous magnetization, which for very small nickel crystallites is assumed to be that of bulk nickel [485 G at 293 K (1 gauss $\triangleq 10^{-4}$ T $= 10^{-4}$ kg s^{-2} A^{-1})] (*14*). Crystallite diameters were derived from such volumes by assuming spherical particles.

Application of this induction-coil technique though ideally suited to such measurements was, however, limited to catalyst metal loadings of more than ca. 2% on high-surface-area carriers. For other preparations the enhanced sensitivity of the Faraday method was used though the initial magnetizations could be derived only from extrapolation. The catalysts for these low-field studies were pretreated and reduced in a quartz reactor prior to degassing (350°C, 2 hr at 10^{-6} Torr) and transferring *in vacuo* into quartz side tubes, which were subsequently sealed off (*in vacuo*).

2. Catalyst Preparation

a. Pretreatment of Carrier

Because of the sensitivity of the Faraday method to the ferromagnetism of trace impurities, various modifications of the highly pure Davison 70 silica carrier, used in catalyst preparation, were washed extensively with hydrochloric acid (4 *M*) until the gel gave a negative test for iron with ammonium thiocyanate solution. The support was then treated with demineralized water until free from chloride ions.

The carriers were dried at 110°C *in vacuo* and calcined for 3 hr at 500°C prior to catalyst preparation. In order to vary the support surface area prehydrothermal treatments of the carrier for 1 hr at 150 and 300°C were applied, generating surface areas of 180 and 19 m^2/g, respectively, in contrast to that of 380 m^2/g for the untreated support. Such procedures imparted to the carriers a field-independent diamagnetic susceptibility, thereby establishing unambiguously the absence of ferromagnetic impurities in the carrier.

b. Catalysts Prepared by Impregnation

The "dry" impregnation method was employed, in which the required amounts of metal in aqueous solution (as nitrates or sulfates) were added to the carrier until it was incipiently wet, using a rotary evaporator and a vacuum of ca. 20 Torr to facilitate penetration of the solution into the pores of the support. Surface moisture was removed by spreading the impregnated support over filter paper prior to drying in a vacuum oven at 100°C for 1 hr. Some preparations were subsequently calcined at 500°C for 3 hr.

c. Catalysts Prepared by Ion Exchange

Silica gel, because of its hydroxylated surface, can act as a cation exchanger, which for transition-metal ions is facilitated by an ammoniacal environment (*26–28*). Therefore, sufficient ammonia hydroxide was added to a nitrate solution of the desired copper and/or nickel concentration(s) until the precipitated hydroxides were redissolved and a small excess of base was present. The carrier was ion-exchanged by stirring it in twice its volume of this ammoniacal solution for 1 to 2 hr prior to filtering and extensive washing with distilled water. (This treatment does not remove the exchanged transition-metal ions.) A total cation-exchange capacity of about 4% wt was found.

d. Catalysts Prepared by Coprecipitation

A solution of copper and nickel nitrate was added with vigorous stirring to a solution of sodium waterglass having a silica content of 14.6%. The pH was adjusted to 10 with concentrated ammonium hy-

droxide and the copper–nickel–silica coprecipitate was formed. Stirring was continued until a homogeneous mass was obtained. This was then filtered and the catalysts were dried and calcined as required.

III. RESULTS

1. Direct Reduction of Nitrates

Figure 2 shows the variation of nickel specific magnetization with applied field for a reduced silica (380 m^2/g) supported copper–nickel nitrate catalyst of ca. 1% total metal loading (curve A′) together with that of the corresponding nickel standard (curve A) after nitrate reduction. The low nickel specific magnetizations in both catalysts are typical of superparamagnetic systems. As expected from the Langevin equation (*14*) a superimposition of magnetizations was observed when plotted against applied field divided by temperature.

As the nickel magnetizations in the bimetallic catalysts were, in all cases, lower than those of the reference preparations,

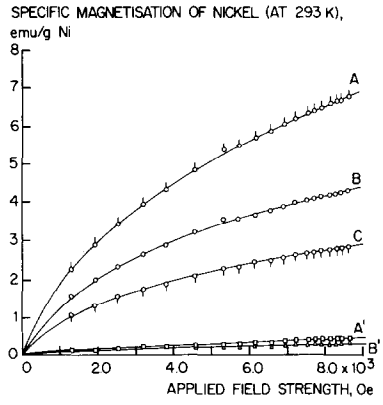

FIG. 2. Specific magnetization of nickel vs applied field strength for a 0.75%wt Cu–0.2%wt Ni and a 0.25%wt Ni-on-silica catalyst. (A) Ni catalyst after reduction at 500°C (16 hr); (B) Ni catalyst as in (A) after hydrogen adsorption (1 hr; 1 bar; 293 K); (C) Ni catalyst as in (B) after oxygen adsorption (1 hr; 1 bar; 293 K); (A′) Cu–Ni catalyst after reduction at 500°C (16 h); (B′) Cu–Ni catalyst as in (A) after hydrogen adsorption (1 hr; 1 bar; 293 K).

we conclude that the decreased nickel magnetic moment of the former is due to copper–nickel alloy formation. An alternative explanation, ascribing the lower magnetization to a decrease in the size of the superparamagnetic nickel particles in the bimetallic sample, is rejected because such a drastic change in particle size would only occur as a result of alloying.

The magnetizations of both the mono- and bimetallic catalysts were decreased upon hydrogen adsorption (curves A to B and A′ to B′, respectively, in Fig. 2). That these magnetization losses in the bimetallic catalysts were due solely to surface nickel and not, for example, produced by the highly dispersed ferromagnetic impurities in copper, as observed by Selwood (*21*), was proved by the fact that a copper/SiO_2 reference sample exhibited a field-independent and constant mass susceptibility before and after hydrogen exposure. Moreover, the agreement between the observed susceptibility (extrapolated to infinite field) of -0.349×10^{-6} cc/g and that expected from component additivity (-0.365×10^{-6} cc/g) suggests that the copper is essentially in the zero-valent state upon reduction of such silica-supported preparations. This conclusion corresponds with results from temperature programmed reduction studies (*29*). The decrease in magnetization caused by hydrogen adsorption was consistently less in the bimetallic samples than in the corresponding nickel-only standard, demonstrating suppressed surface nickel availability due to alloying. Estimates of nickel surface areas (and of particle sizes) in the nickel-only catalysts can be derived from the magnetization changes by assuming that every surface nickel atom adsorbs a hydrogen atom and has its magnetic moment erased. The nickel surface areas evaluated as described elsewhere (*30,31*) are only qualitative, however, as hydrogen adsorption produces a smaller nickel "particle," which in its turn contributes to the decrease in magnetization. From the mag-

netization changes (at 8 kOe, for example) such apparent nickel specific surface areas are calculated. The nickel particle sizes thus obtained for the high-surface-area (380 m^2/g) silica (assuming that the apparent nickel specific surface area represents 80% of the total) appear to be independent of the metal loading and reduction temperature adopted (Table 1). The low-field (initial slope) estimates of larger crystallite sizes show a relatively narrow range of particle sizes in these reduced high-surface-area catalysts. That some of the nickel crystallites were indeed larger than those given by hydrogen adsorption was demonstrated by incomplete erasure of nickel magnetization upon exposure to oxygen (e.g., curve C in Fig. 2), which is corrosively chemisorbed, thereby "demetallizing" nickel to about 2.0 nm in depth (*32*).

Decreasing the carrier surface area to 19 m^2/g results in a marked increase of nickel magnetization in such reduced nitrate catalysts (Table 1), which is illustrative of much poorer metal dispersion. This was confirmed by the greatly diminished nickel surface areas in these low-surface-support catalysts, where alloying was also identified by the reduced magnetization of the bimetallic sample (Table 1).

2. Reduction of Nitrates after Calcination

Much larger particles (and hence magnetizations) were obtained when the nitrates

TABLE 1
MAGNETIC ANALYSIS OF SUPPORTED Cu–Ni CATALYSTS AFTER NITRATE DRYING (WITH OR WITHOUT CALCINATION)

Metal loading (%wt)					$\sigma^{Ni}_{(8\,kOe,\,293\,K)}$ (emu/g)		Apparent nickel specific surface area (m^2/g)		Ni particle size in Ni cat. (nm)	
Nickel standard	Bimetallic Cu	Bimetallic Ni	Support area (m^2/g)	Treatment[a] (gas/°C)	Nickel standard	Bimetallic catalyst	Nickel standard	Bimetallic catalyst	Low field	H_2ADS[b]
1.63	6.49	1.94	380	H_2 400	2.1	0.4	578	421	8.0[c]	1.0
				H_2 500	2.8	0.6	418	412		1.3
0.52	0.38	0.57	380	H_2 400	2.3	0.7	432	402	1.5[d]	1.4
				H_2 500	2.8	0.8	441	323	1.6[d]	1.3
0.25	0.80	0.29	380	H_2 500	6.6	0.4	249	201	4.0[d]	2.3
0.25	0.78	0.26	19	H_2 500	30.2	7.8	42	15	20.7[c]	13.3
0.25	0.75	0.24	380	calcined[e] + H_2 500	44.8	3.5	42	11	9.0[d]	13.2
2.50	5.79	2.20	380	calcined[e] + H_2 400	51.6	3.9	29	28	11.3[c]	19.6
2.50	5.60	2.20	180	calcined[e] + H_2 400	51.8	8.3	27	14	7.8[c]	21.0
2.50	7.40[f]	2.20	180	calcined[e] + H_2 400	51.8	8.8	27	11	15.7[d]	21.0
2.50	4.17	2.09	180	calcined[e] + H_2 400 (2 hr)	44.6	10.8	27	11	14.6[d]	21.0

[a] 16 hr treatment time unless otherwise stated.
[b] From apparent nickel specific surface area.
[c] Low-field induction method.
[d] Faraday balance estimate.
[e] 3 hr in air at 500°C.
[f] Successive impregnation –Cu salt first.

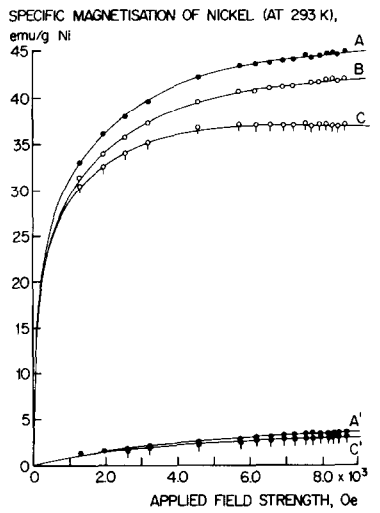

FIG. 3. Specific magnetization of nickel vs applied field strength for a 0.75%wt Cu–0.24%wt Ni and a 0.25%wt Ni-on-silica catalyst after calcination (500°C, 3 hr) and reduction at 500°C for 16 hr. (A) Ni catalyst after reduction; (B) Ni catalyst as in (A) after hydrogen adsorption; (C) Ni catalyst as in (A) after oxygen adsorption; (A′) Cu–Ni catalyst after reduction; (C′) Cu–Ni catalyst as in (A′) after oxygen adsorption.

on the high-surface-area silica (380 m^2/g) were precalcined prior to reduction (Fig. 3; Table 1). Indeed the degree of metal dispersion was so low that the specific magnetizations of the nickel reference catalysts approached the saturation value of the bulk element. Alloying in the bimetallic catalysts can again be concluded from their suppressed nickel magnetizations (compare curves A and A′ in Fig. 3). We can affirm further, from this large decrease of magnetization compared to noncalcined catalysts (Fig. 2, curves A and A′), that more effective copper–nickel alloying has occurred. The very small decrease in the nickel specific magnetization of the bimetallic catalyst caused by oxygen adsorption also supports this view, as do the results of other catalytic studies (*33*).

The magnetic and surface properties of these calcined catalysts after reduction were essentially independent of reduction and metal loading conditions. The reduced effect of oxygen in demagnetizing the nickel is consistent with the occurrence of poorly dispersed metal particles.

Reduction of the support surface area to 180 m^2/g produces a further decrease in nickel surface exposure and dispersion of alloy particles. These parameters are essentially unaffected by the mode of salt impregnation (successive or common), metal loadings and reduction conditions of time and temperature.

3. Reduction of Ion-Exchanged Catalysts

The lower nickel specific magnetizations (relative to the corresponding nickel standard) of reduced (ca. 1% loaded) copper–nickel ion-exchanged on silica (380 m^2/g) catalysts produce highly dispersed alloy particles (Table 2). The surface of nickel in these samples is, hence, lower than in the corresponding nickel-only standard. Such alloying is, however, also nonuniform, as demonstrated by the residual superparamagnetism of this Cu-rich bimetallic catalyst, its sensitivity to hydrogen and the temperature dependence of the observed catalyst mass susceptibility, which differs from that expected for a homogeneous solid solution alloy on the carrier.

The data of Table 2 suggest that the overall nature of bimetallic alloying was comparable to that of reduced nitrates on the same support, though the induction coil estimate of 1.7 nm particles suggests superior metal dispersion (*26*). Moreover, the magnetic properties of these reduced ion-exchanged catalysts were independent of the mesh size of the carrier used.

4. Reducibility of Silica-Supported Nickel Catalysts

It has been reported that when some metals occur in dilute form on high-surface-area supports (including silica) they do not exist in the zero-valent state after hydrogen treatment (*34,35*). As these observations are pertinent to this work, we report here magnetic studies of nickel re-

TABLE 2
MAGNETIC ANALYSIS OF SUPPORTED Cu–Ni AND Ni CATALYSTS AFTER ION EXCHANGE AND REDUCTION

Metal loading (%wt)					$\sigma^{Ni}_{(8\,kOe,293\,K)}$ (emu/g)		Apparent nickel specific surface area (m^2/g)		Ni particle size in Ni cat. (nm)	
Nickel standard	Bimetallic Cu	Bimetallic Ni	Support[a] area (m^2/g)	Treatment[b] (gas/°C)	Nickel standard	Bimetallic catalyst	Nickel standard	Bimetallic catalyst	Low field	H_2ADS[c]
2.41	1.67	2.29	380	H_2 400	2.38	0.84	471	228	1.7[d]	1.2
				H_2 500	3.20	1.62	508	405	1.6[e]	1.1
0.26	0.77	0.29	380	H_2 400	2.61	0.39	450	92	1.4[e]	1.2
				H_2 500	3.67	0.26	462	304	1.6[e]	1.2
0.25	0.85	0.28	380[f]	H_2 400	2.13	0.56	457	65	1.3[e]	1.2
				H_2 500	3.20	0.44	469	184	1.5[e]	1.2

[a] Support mesh size 0.42–0.18 mm.
[b] 16 hr treatment time.
[c] From apparent nickel specific surface area.
[d] Low-field induction method.
[e] Faraday balance estimate.
[f] Support mesh size 0.18–0.07 mm.

duction in catalysts where the metal concentration is less than 3% on a high-surface-area (380 m^2/g) Davison 70 silica. The magnetic properties of some nickel–silica catalysts were determined in their vacuum-sealed SiO_2 tubes at room temperature with the low-field induction coil. The dependence of the nickel specific magnetization on field strength for a 0.27% nickel catalyst after impregnation and reduction at 500°C is given by curve A in Fig. 4. These specific magnetizations are considerably lower than the corresponding values for a very finely divided nickel powder, shown in curve B.

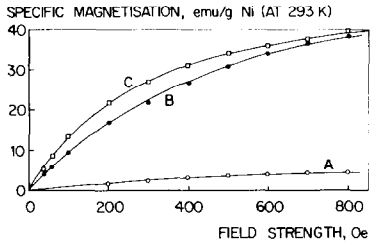

FIG. 4. Magnetization of a 0.27%wt Ni-on-silica catalyst. (A) Catalyst after 16 hr reduction at 500°C; (B) nickel powder standard; (C) catalyst as in (A) after vacuum sintering at 800°C.

This finding may be interpreted as being due either to incomplete reduction, the extent of which may vary with nickel concentration, or to the very high degree of nickel dispersion engendering this superparamagnetic profile.

To distinguish between these alternatives the catalyst was further heated in the vacuum-sealed quartz tube at 800°C for several hours to induce metal crystallite growth. The magnetizations were thereby increased (Fig. 4, curve C) and indeed exceeded those of the finely divided nickel powder studied. We therefore conclude that the catalyst was well reduced and that the low magnetization value found after the reduction step was due to crystallite-size effects.

The apparent saturation magnetization per gram of nickel in the sintered (0.27% Ni) catalyst was estimated from a plot of the reciprocal specific magnetization against (reciprocal field strength)$^{0.9}$ and by extrapolating to infinite field (*24*) (Fig. 5).

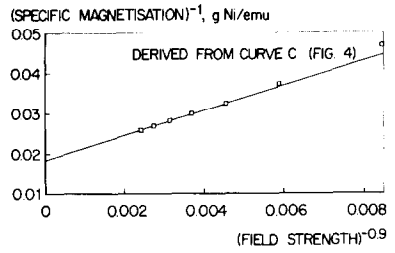

FIG. 5. Reciprocal of nickel specific magnetization vs (applied field)$^{-0.9}$ of a 0.27%wt Ni-on-silica catalyst.

An apparent saturation magnetization of 54.40 emu/g was observed, which compared closely with that measured for the nickel powder. From this we infer that all the nickel of the supported catalyst existed in the free metallic state after reduction. Estimates of nickel crystallite sizes from the initial slope of these specific-magnetization-against-field profiles show that sintering at 800°C clearly leads to an at least threefold increase in crystallite size, which is responsible for the enlarged apparent saturation magnetizations.

Table 3 shows that other silica-supported nickel catalysts can likewise be completely reduced by hydrogen at 500°C and indeed these findings were confirmed by temperature programmed reduction (*29*) of such nickel (and copper) samples. Moreover, calcination of the dried nitrate followed by reduction without a subsequent sintering step engenders an apparent saturation magnetization of 54.35 emu/g. Thus, the calcination step is responsible for a very poor dispersion of metallic nickel on reduction.

5. Reduction of Sulfate Catalysts

The diminished nickel specific magnetization-vs-field profile of a reduced copper–nickel sulfate on silica catalyst (curve A′; Fig. 6), relative to that of the nickel reference standard (curve A), suggests that considerable alloying has taken place as the residual (diamagnetic) sulfur level on the two catalysts was equivalent.

Support for alloy formation in such reduced sulfate catalysts was given by moving-film X-ray evidence of successive formation of Cu- (ca. 90%wt) and Ni- (ca. 74%wt) rich alloys on *in situ* hydrogen treatment of the catalyst up to 500°C.

The samples obtained by reducing sulfates show, however, a very low response to magnetization upon hydrogen adsorption. In the case of the Ni standard, the low-field (Faraday) estimate of 2.8 nm particle size should engender a much larger magnetization change on hydrogen adsorption than that observed (curves A and B in Fig. 6).

In the copper–nickel catalyst the magne-

TABLE 3

APPARENT SATURATION MAGNETIZATION (AT 293 K) OF HIGH-SURFACE-AREA SILICA-SUPPORTED NICKEL CATALYSTS AFTER VACUUM SINTERING AT 800°C

Nickel loading (%wt)	Preparation method	Reduction temp[a] (°C)	Crystallite size (nm); sintering		Apparent saturation magnetization[b]
			Before	After	
0.27	Impregnation	500	4.0	11.0	54.40
2.19		400	8.0	23.0	54.00
2.31[c]	Calcination	400	11.5	—	54.35
0.25	Ion exchange	500	—	7.5	52.60
2.53		500	1.7	12.0	53.76

[a] 16 hr reduction time.

[b] Apparent saturation magnetization of bulk nickel 54.39 (293 K).

[c] Not sintered after reduction.

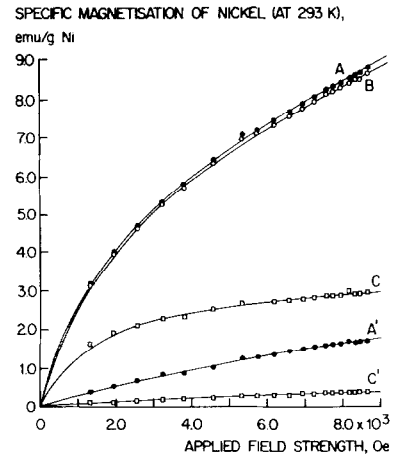

FIG. 6. Specific magnetization of Ni vs applied field strength for a 0.34%wt Cu–0.68%wt Ni and a 0.38%wt Ni-on-silica (380 m^2/g) catalyst after sulfate impregnation, drying and reduction (500°C, 16 hr). (A) Ni catalyst after reduction; (B) Ni catalyst as in (A) after hydrogen adsorption; (C) Ni catalyst as in (A) after oxygen adsorption; (A') Cu–Ni catalyst after reduction; (C') Cu–Ni catalyst as in (A') after oxygen adsorption.

tization-field profiles were even indistinguishable for the freshly reduced and the hydrogen-exposed state. This anomalously low-surface-nickel availability for gas adsorption probably arises from the sulfate-reduction method producing highly dispersed but partially sulfided nickel particles.

That the metallic nickel is sulfided rather than existing entirely as nickel sulfide (Ni_3S_2) is demonstrated by the dilute ferromagnetism observed for the catalyst in contrast to the dia- or paramagnetic behavior expected for the bulk sulfide on the silica carrier. We can affirm, however, that the surface, and consequently catalytic, properties of the sulfate-doped catalysts are dictated by this residual sulfur after reduction—a conclusion strongly supported by *n*-hexane dehydrocyclization work (*33*).

6. Coprecipitated Catalysts

The extent of alloying in the reduced copper–nickel coprecipitated catalyst appears to be small as the low-field specific magnetization is slightly less than that of the corresponding monometallic reference standard. Dried and air-calcined samples were examined by X-ray powder diffractometry after hydrogen reduction at 400°C for 4 hr. There was virtually no alloying as the X-ray pattern showed separate copper and nickel nonalloyed phases. Reduction of the dried coprecipitated catalyst in the high-temperature Guinier camera showed that the copper phase crystallized at about 180°C and the nickel at about 350°C. Such coprecipitation methods are therefore completely unsuitable for the formation of homogeneous copper–nickel alloys.

7. Detection of Supported Copper–Nickel Alloying by Ferromagnetic Resonance

Ferromagnetic resonance (FMR) has been used in the study of the adsorption of hydrogen and other gases on nickel–silica catalysts (*36*). Such adsorbates engendered, in general, a decrease in the intensity and/or line width of the usually large and broad nickel FMR signals. These changes in the FMR of nickel are caused by the removal of surface electron spins and/or a decrease in the inherent magnetocrystalline anisotropy of the nickel particles. As the specific magnetization of nickel is also decreased on interaction with copper on silica supports, FMR can also be useful in the detection of alloying in highly dispersed supported copper–nickel samples, thereby complementing the magnetostatic method.

Therefore, various supported copper–nickel catalysts (together with the corresponding nickel monometallic standards) were prepared, reduced, degassed (at 350°C for 2 hr to remove residual adsorbed hydrogen) and transferred *in vacuo* into FMR sample tubes, which were subsequently sealed off. Catalyst details and treatment conditions are listed in Table 4, together with details of the FMR spectra, all of which were obtained at 20°C.

TABLE 4
FERROMAGNETIC RESONANCE RESULTS FROM Cu–Ni AND Ni-ON-SILICA CATALYSTS

Catalyst description	Metal loading (%wt)	Surface area of silica support (m^2/g)	FMR results: Signal height (arb. units)	FMR results: Signal line width (arb. units)
Calcined (500°C, 3 hr)	Ni 2.5		90	122
+Reduced (400°C, 16 hr)	Cu 7.5, Ni 2.5	19	86	81
Calcined (500°C, 3 hr)	Ni 5.0		97	150
+Reduced (400°C, 16 hr)	Cu 5.0, Ni 5.0	380	26	42
NO_3-impregnated	Ni 2.5		89	197
+Reduced (400°C, 16 hr)	Cu 7.5, Ni 2.5	380	3	39
Ion-exchanged	Ni 3.0		43	130
+Reduced (500°C, 16 hr)	Cu 2.0, Ni 3.0	380	12	115
Coprecipitated	Ni 5.3		88	114
+Reduced (440°C, 16 hr)	Cu 5.3, Ni 5.3	—	59	103

As an example, two spectra are shown in Fig. 7. One is of a copper-nickel ion-exchanged catalyst and the other of the corresponding monometallic nickel reference standard. There is clearly a decrease in the intensity of the nickel FMR signal in the bimetallic preparation, which is illustrative of alloying. Comparison of FMR spectra intensities and line widths (Table 4) of all the other copper–nickel and nickel reference catalysts demonstrated, in general, a decrease in the magnitude of these parameters in the spectra of the bimetallic samples. Therefore, we conclude that the FMR technique can yield rapid evidence of highly dispersed copper–nickel alloying on a carrier.

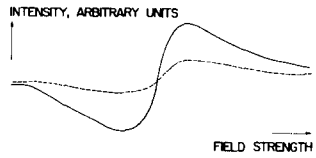

FIG. 7. FMR spectra at 20°C of a 2%wt Cu–3%wt Ni-on-silica catalyst (---) and a 3%wt Ni-on-silica catalyst (—) both after ion exchange and reduction (500°C, 16 hr).

IV. DISCUSSION

The magnetostatic (and resonance) methods have demonstrated clearly an ability to identify monometallic reducibility and alloying in highly dispersed bimetallic particles, thereby complementing other studies in this field (*29,33,37–39*). Moreover, these magnetization studies have revealed that all the catalyst preparation methods used engender bimetallic interaction except those from the coprecipitation route. Some doubt has, however, been expressed over the complete reducibility of unsupported copper–nickel alloys due to water "encapsulation" (*40*). We believe from temperature programmed reduction studies (*29*) that total alloy reduction does occur on silica by 500°C.

The residual superparamagnetism of completely reduced copper-rich catalysts, however, and the sharp decrease in magnetization caused by hydrogen adsorption show that some bimetallic particles contain more nickel than the average of the sample and that alloying over the catalyst as a whole cannot be described completely in

terms of either the two-phase (cherry) or random solid substitution models. Further evidence of nonuniform alloying was provided by the observed catalyst magnetic susceptibilities being higher than those calculated on an additive basis for the homogeneous alloy (*41*) on the same support.

The information obtained in this work from magnetic data is limited by the fact that nonuniform alloying and dispersion will both affect the magnetization curves in a similar manner. In real supported systems the particles have neither the same size nor (in bimetallic catalysts) uniform composition but a range of these will be present in any given sample with *a priori* unknown distribution functions. A separation of these two effects might, in principle, be obtained by including measurements at extremely low temperatures (ca. 0 K) where it is believed that there is no influence of particle size on nickel magnetization (*14*). Such studies for silica-supported copper–nickel catalysts have indeed been recently reported (*42*) and the results confirm our conclusion that the cherry model does not apply to supported systems.

With finely dispersed bimetallic systems, it can be shown statistically that for a 75%wt Cu–25%wt Ni sample with 1.0 nm particles (ca. 100 atoms) the relative probability of finding particles having 60% Cu, 40% Ni is less than 0.5% of those with a composition of 75% Cu, 25% Ni. The catalyst mass susceptibility observed for the 1% metal catalyst (mean $\chi_{catalyst}$ is -0.235×10^{-6} cc/g from the direct reduction of the nitrates) exceeds that expected (-0.357×10^{-6} cc/g) even if *all* the particles were of 60% Cu, 40% Ni composition.

In other words, the observed catalyst magnetic susceptibility exceeds that expected from a supported system where a statistical distribution of metal particle compositions exists. We affirm, therefore, that the alloying observed in this (and other) finely divided catalysts was heterogeneous in the sense that the distribution of composition over all the individual particles deviated from the ideal case, even when statistical variations of particle compositions are considered.

This conclusion was supported by the direct reduction of the bimetallic nitrates revealing an X-ray diffraction pattern of symmetrical peaks for free copper only. This evidently proves an incomplete engagement of this metal in alloy formation.

The present work has further shown that silica supports clearly allow complete reduction of the metal particles, confirming independent results that hydrogen treatment of such impregnated or ion-exchanged precursors causes no deep interaction between nickel (and presumably copper) and the support (*43*). Bimetal impregnates on low-surface-area supports could therefore be of potential value for the rapid manufacture of supported alloys. The degree of metal dispersion is, for the copper–nickel system, strongly decreased if a calcination step is incorporated into the catalyst preparation (Table 1) and this is confirmed by alloying being detectable by X-ray diffraction. Even under these circumstances some nonalloyed copper was always present, as shown in Fig. 8. When the composition of the alloy found is calculated from the position of the X-ray diffraction peak, using the data of Coles (*44*), it differs significantly from the overall composition calculated from the metal loadings. This correspondence is better, however, at higher nickel relative loadings. Such an improvement can be correlated with an enhanced miscibility of CuO in NiO (ca. 35%mol max) compared with that of NiO in CuO (ca. 5%mol max) (*45*) Indeed, the calculated compositional assignment of the alloy peaks in the 7.5%wt Cu:2.5%wt Ni and 5%wt Cu: 5%wt Ni catalysts in Fig. 8 corresponds approximately with this maximum

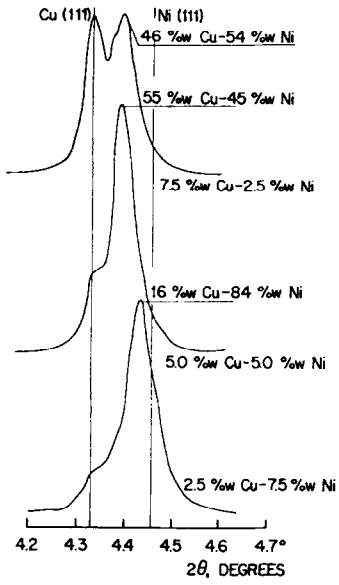

FIG. 8. X-Ray spectra of calcined Cu–Ni-on-silica catalysts after reduction at 400°C.

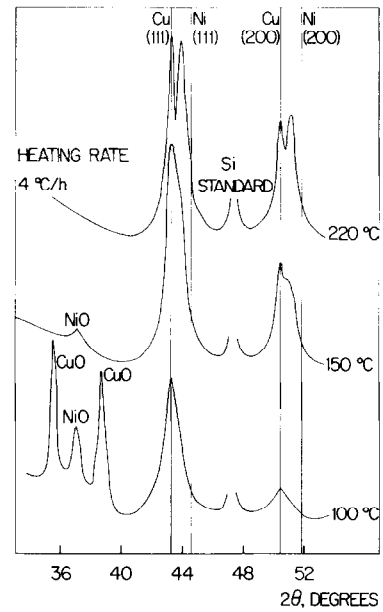

FIG. 9. *In situ* X-ray study of a calcined 5.79%wt Cu–2.22%wt Ni-on-silica catalyst heated in hydrogen.

Ni atom replaceability (ca. 35%) by copper. We conclude, therefore, that the extent of ultimate homogeneity in alloying in these precalcined samples after reduction is controlled by such oxide phase miscibilities. Moreover, the reduction of such precalcined catalysts was also continuously monitored by a high-temperature moving film Guinier X-ray technique where the alloy reflection (ca. 60%at. Ni, 40%at. Cu) appeared at higher hydrogen treatment temperatures after the development of free copper. Such stepwise product formation occurred with the preferential removal of the copper oxide reflection (Fig. 9).

The hydrogen treatment of nitrate-containing precursors also involves reduction of the anion with the consequent exothermicity of the reaction. The heat liberated, however, in nitrate reduction, involving three moles of hydrogen (*29*), could generate a maximum adiabatic temperature rise of only about 100°C in such 10% metal-loaded catalysts, whereas efficient heat dissipation into the highly conducting reduction gas occurs in the reduction systems used. We conclude, therefore, that the highly exothermic nature of nitrate reduction will not engender significant catalyst particle sintering in this case and, moreover, our finding of such completely reducible but highly dispersed preparations matches those of similar studies (*30,31*). It would seem that incorporation of a precalcination step yields samples containing more crystalline precursors than the dried-only salts. Precalcination could be an initial metal aggregation step, resulting in more poorly dispersed, but more efficiently alloyed, copper–nickel catalysts on reduction.

The reducibility of the metal precursors can govern the nature of the catalysts as, for example, in the hydrogen treatment of sulfate-containing preparations. Here the residual sulfur alters the properties of the metallic nickel when tested for the dehydrocyclization of *n*-hexane, suppressing cracking and low-temperature isomerization (*33*).

Despite most of the silica-supported components studied being completely reducible, they were not reduced simultaneously (*29*). This was clearly revealed in the reduction of copper and nickel oxides from precalcined Cu-rich catalysts. The increasing miscibility of the former oxide in the latter at high relative nickel loadings clearly favored an enhanced bimetallic interaction (*46*) (see Fig. 8).

We conclude, therefore, that a prerequisite for homogeneous and highly dispersed alloying on carriers in general is a complete and simultaneous bimetallic interplay resulting from an intimate emplacement and concomitant reducibility of the metals. Favorable bimetallic systems, therefore, could be those where metal–metal bonds occur (in complexes, for example), which are directly reducible or, alternatively, form mutually miscible oxides having the same free energy of reduction.

ACKNOWLEDGMENTS

The authors thank Messrs. J. Jonk and H. B. M. Wolters for X-ray diffraction work and Dr. M. M. P. Janssen for his stimulating remarks and suggestions. The constructive comments of a referee are also gratefully acknowledged.

REFERENCES

1. Flank, W. H., and Beachell, H. C., *J. Catal.* **8,** 316 (1967).
2. Van Ham, N. H. A., Nieuwenhuys, B. E., and Sachtler, W. M. H., *J. Catal.* **20,** 408 (1971).
3. Gharpurey, M. K., and Emmett, P. H., *J. Phys. Chem.* **65,** 1182 (1961).
4. Best, R. J., and Russel, W. W., *J. Amer. Chem. Soc.* **76,** 838 (1954).
5. Sachtler, W. M. H., and Van der Plank, P., *Surface Sci.* **18,** 62 (1969).
6. Cadenhead, D. A., Wagner, N. J., and Thorp, R. L., *Proc. Int. Congr. Catal., 4th, 1968* **1,** 341 (1971).
7. Carr, P. F., and Clarke, J. K. A., *J. Chem. Soc. A.* **1971,** 985.
8. Ponec, V., and Sachtler, W. M. H., *Proc. Int. Congr. Catal., 5th, 1972* **2,** 645 (1973).
9. Swift, H. E., Lutinski, F. E., and Kehl, W. L., *J. Phys. Chem.* **69,** 3268 (1965).
10. Reynolds, P. W., *J. Chem. Soc.* **1950,** 242.
11. Delgass, W. N., Hughes, T. R., and Fadley, C. F., *Catal. Rev.* **4,** 179 (1970).
12. Bouwman, R., Biloen, P., and Robertson, S. D., unpublished data.
13. Ahearn, S. A., Martin, M. J. C., and Sucksmith, W., *Proc. Roy. Soc., Ser. A* **248,** 145 (1958).
14. Selwood, P. W., "Adsorption and Collective Paramagnetism." Academic Press, New York, 1962.
15. Kittel, C., *Phys. Rev.* **70,** 965 (1946).
16. Broeder, J. J., Van Reijen, L. L., and Korswagen, A. R., *J. Chim. Phys.* **54,** 37 (1957).
17. Sachtler, W. M. H., and Dorgelo, G. J. H., *J. Catal.* **4,** 654 (1965).
18. Sachtler, W. M. H., and Jongepier, R., *J. Catal.* **4,** 665 (1965).
19. Elford, L., Müller, F., and Kubaschewski, O., *Ber. Bunsengas. Phys. Chem.* **73,** 601 (1969).
20. Ollis, D. F., *J. Catal.* **23,** 131 (1971).
21. Selwood, P. W., "Magnetochemistry," 2nd ed., p. 27. Wiley (Interscience), New York, 1956.
22. Morris, B. L., and Wold, A., *Rev. Sci. Instrum.* **39,** 1937 (1968).
23. Earnshaw, A., "Introduction to Magnetochemistry." Academic Press, London, 1968.
24. Heukelom, W., Broeder, J. J., and Van Reijen, L. L., *J. Chim. Phys.* **51,** 473 (1954).
25. Dietz, R. E., and Selwood, P. W., *J. Chem. Phys.* **51,** 270 (1961).
26. Benesi, H. A., Curtis, R. M., and Studer, H. P., *J. Catal.* **10,** 328 (1968).
27. Hathaway, B. J., and Lewis, C. E., *J. Chem. Soc. A* **1969,** 1176.
28. Poltorak, O. M., and Boronin, V. S., *Russ. J. Phys. Chem.* **39,** 781 (1965).
29. Robertson, S. D., McNicol, B. D., de Baas, J. H., Kloet, S. C., and Jenkins, J. W., *J. Catal.* **37,** 424 (1975).
30. Carter, J. L., Cusumano, J. A., and Sinfelt, J. H., *J. Phys. Chem.* **70,** 2257 (1966).
31. Carter, J. L., and Sinfelt, J. H., *J. Phys. Chem.* **70,** 3003 (1966).
32. Janssen, M. M. P., *J. Appl. Phys.* **41,** 384 (1970).
33. Robertson, S. D., Helle, J. N., Hendriks, P. A. J. M., and Sachtler, W. M. H., unpublished data.
34. Voge, H. H., and Atkins, L. T., *J. Catal.* **1,** 171 (1962).
35. Holm, V. C. F., and Clark, A., *J. Catal.* **11,** 305 (1968).
36. Andreev, A. A., and Selwood, P. W., *J. Catal.* **8,** 375 (1967).
37. Reman, W. G., Ali, A. H., and Schuit, G. C. A., *J. Catal.* **20,** 374 (1971).
38. Soma-Noto, Y., and Sachtler, W. M. H., *J. Catal.* **32,** 315 (1974).

39. Cormack, D., Thomas, D. H., and Moss, R. L., *J. Catal.* **32,** 492 (1974).
40. Scholtus, W. A., and Hall, W. K., *Trans. Faraday Soc.* **59,** 969 (1963).
41. Pugh, E. W., and Ryan, F. M., *Phys. Rev.* **111,** 1038 (1958).
42. Dalmon, J. A., Martin, G. A., and Imelik, B., *Surface Sci.* **41,** 587 (1974).
43. Dzis'ko, V. A., Noskova, S. P., Karachiev, L. G., Borisova, M. S., Bolgova, V. G., and Tyulikova, T. Y. A., *Kinet. Catal.* **13,** 327 (1972).
44. Coles, B. R., *J. Inst. Metals* **84,** 346 (1956).
45. Bertaut, F., and Delorme, C., *C. R. Acad. Sci.* **223,** 356 (1951).
46. Hall, W. K., and Alexander, L., *J. Phys. Chem.* **61,** 242 (1957).